# Diffuse supernova neutrino background as a probe of late-time neutrino mass generation

André de Gouvêa, 1,\* Ivan Martinez-Soler, 2,† Yuber F. Perez-Gonzalez, 3,‡ and Manibrata Sen, 1 Northwestern University, Department of Physics and Astronomy, 2145 Sheridan Road, Evanston, Illinois 60208, USA
2 Department of Physics and Laboratory for Particle Physics and Cosmology, Harvard University, Cambridge, Massachusetts 02138, USA
3 Institute for Particle Physics Phenomenology, Durham University, South Road, Durham DH1 3EL, United Kingdom
4 Max-Planck-Institut für Kernphysik, Saupfercheckweg 1, 69117 Heidelberg, Germany

(Received 7 June 2022; accepted 1 November 2022; published 22 November 2022)

The relic neutrinos from old supernova explosions are among the most ancient neutrino fluxes within experimental reach. Thus, the diffuse supernova neutrino background (DSNB) could teach us if neutrino masses were different in the past (redshifts  $z \lesssim 5$ ). Oscillations inside the supernova depend strongly on the neutrino mass-squared differences and the values of the mixing angles, rendering the DSNB energy spectrum sensitive to variations of these parameters. Considering a purely phenomenological parametrization of the neutrino masses as a function of redshift, we compute the expected local DSNB spectrum here on Earth. Given the current knowledge of neutrino oscillation parameters, especially the fact that  $|U_{e3}|^2$  is small, we find that the  $\nu_e$  spectrum could be significantly different from standard expectations if neutrinos were effectively massless at  $z \gtrsim 1$  as long as the neutrino mass ordering is normal. On the other hand, the  $\bar{\nu}_e$  flux is not expected to be significantly impacted. Hence, a measurement of both the neutrino and antineutrino components of the DSNB should allow one to test the possibility of recent neutrino mass generation.

DOI: 10.1103/PhysRevD.106.103026

#### I. INTRODUCTION

The discovery of neutrino oscillations in the last century established without a doubt that neutrinos are massive. Neutrino oscillations provide precise information on the neutrino mass-squared differences but are independent from the absolute masses of the neutrinos. Data from neutrino oscillation experiments can be used to constrain the sum of the neutrino masses to  $\sum m_i \gtrsim 0.058$  eV, i=1,2,3 in the case of the normal mass ordering (NO)  $(m_3 > m_2 > m_1)$  or  $\sum m_\nu \gtrsim 0.1$  eV in the case of the inverted mass ordering (IO)  $(m_2 > m_1 > m_3)$  [1]. A kinematic upper bound to the neutrino masses, mostly model independent, comes from the Karlsruhe Tritium Neutrino Experiment (KATRIN) [2,3], which measures the beta-decay spectrum of tritium atoms.

Published by the American Physical Society under the terms of the Creative Commons Attribution 4.0 International license. Further distribution of this work must maintain attribution to the author(s) and the published article's title, journal citation, and DOI. Funded by SCOAP<sup>3</sup>. KATRIN is sensitive to a linear combination of the neutrino masses; their most recent analysis yields an upper limit of  $\sum_i \sqrt{|U_{ei}|^2 m_i^2} < 0.9$  eV (90% confidence level) [3]. The  $U_{ei}$ , i=1,2,3 elements of the mixing matrix are measured with good precision by neutrino oscillation experiments  $|U_{e1}|^2 \sim 0.7$ ,  $|U_{e2}|^2 \sim 0.3$ , and  $|U_{e3}|^2 \sim 0.02$  [4].

The most stringent bounds on neutrino masses come from indirect measurements that rely on their effect on cosmological observables. Massless neutrinos are hot dark matter candidates and mediate a "washing out" of small-scale perturbations in the early Universe. Observations of the cosmic microwave background (CMB) by the *Planck* satellite, combined with gravitational lensing data, baryon acoustic oscillations (BAOs), and large-scale structure limit the sum of neutrino masses  $\sum_i m_i < 0.13 \text{ eV}$  [5]. Excluding BAOs, this limit relaxes to  $\sum_i m_i < 0.24 \text{ eV}$  [6]. Adding Lyman alpha data and CMB temperature and polarization data to the lensing and the BAO data further improves the bound to 0.09 eV [7].

On the theoretical front, extending the standard model (SM) to incorporate neutrino masses has been a topic of intense research. The idea, if neutrinos are Majorana fermions, is to augment the SM in a way so as to generate the effective Weinberg operator (LH)(LH) [8], where L is

degouvea@northwestern.edu

imartinezsoler@fas.harvard.edu

yuber.f.perez-gonzalez@durham.ac.uk

<sup>§</sup>manibrata@mpi-hd.mpg.de

the lepton doublet containing the neutrino, and H is the Higgs doublet. Popular mechanisms like the seesaw models, radiative mass models, and several others rely on the introduction of new degrees of freedom at relatively highenergy scales (see, for example, [9] and references therein). These new massive particles typically decouple from the cosmic plasma in the very early Universe and hence do not alter its evolution.

All current evidence of nonzero neutrino masses arises from experiments at redshift z = 0. In some sense, the "oldest" measurements of the nonzero nature of neutrino masses comes from solar neutrinos. Data from cosmology do not preclude a zero value of neutrino mass but only provide upper limits; the vanilla  $\Lambda$  cold dark matter cosmology is perfectly consistent with zero neutrino masses [6]. As a result, scenarios where neutrinos are massless in the early Universe and gain mass only after recombination are not ruled out. Models predicting a late-time neutrino mass generation rely on time-varying neutrino masses arising out of the neutrino coupling to some time-varying scalar field [10–12], a late-time cosmic phase transition [13], or the gravitational anomaly [14]. Using a combination of CMB temperature and polarization power spectra, plus lensing data, the authors of [13] explored models where the neutrino masses are redshift dependent. They report a slight preference for models of late-time neutrino mass generated by a cosmic phase transition. In this scenario, due to the nontrivial dynamics of the phase transition, the bound on the current sum of neutrino masses is significantly weaker,  $\sum m_{\nu}(z=0)$  < 4.8 eV at 95% CL. In a follow-up work [15], the authors extracted the best-fit values of the neutrino masses as a function of redshift in a model-independent manner, using CMB and BAO data and data from Type-IA supernovae (SNe), and found a significantly weaker bound,  $\sum_{i} m_{\nu_i}(z=0) < 1.46$  eV (95% CL). These looser bounds indicate, for example, that the hypothetical discovery of nonzero neutrino masses in future laboratory experiments [16] would be consistent with bounds from cosmic surveys if we allow for late-time neutrino masses.

The CMB probes high redshifts ( $z \sim 1000$ ), and one may wonder if there are other probes capable of testing the hypothesis that neutrino mass generation occurs at much smaller redshifts. The answer to this question may lie in the diffuse supernova neutrino background (DSNB), a sea of MeV neutrinos emerging from all supernova (SN) explosions in the Universe since the moment of the first stars ( $z \lesssim 5$  is usually considered as a benchmark value) [17,18]. This upper value is somewhat vaguely defined since it does not affect the DSNB spectra in the observable window. This isotropic, time-independent flux of neutrinos can be computed with precise knowledge of the underlying cosmology and the rate at which SNe happen in the Universe. The DSNB can be used as an excellent astrophysical laboratory to probe fundamental particle physics [19–21].

The DSNB flux depends on whether the neutrinos are massive because of neutrino oscillations. For massless neutrinos, flavor eigenstates trivially coincide with mass eigenstates and will not undergo oscillations. However, the picture changes if the neutrinos acquire mass at a certain redshift. This leads to a scenario where the neutrino flavor and mass eigenstates are identical before a certain redshift (hence the mixing matrix is diagonal) and, as soon as they develop a nonzero mass, these two bases no longer coincide. This impacts the DSNB flux that arrives at Earth in a nontrivial way. Neutrinos that were massless at the time of production would not suffer the usual effects that arise from neutrino oscillations inside the SN. As a result, we expect the net DSNB flux to be altered compared to what is predicted in the standard scenario.

The detection of an altered DSNB flux can be used to probe such scenarios of late neutrino mass generation. The Super-Kamiokande (SK) experiment [22], enriched with gadolinium, is ready to search for the DSNB and is expected to establish its existence within a decade [23]. Several upcoming experiments like Hyper-Kamiokande (HK) [24], the Jiangmen Underground Neutrino Observatory (JUNO) [25], and the Deep Underground Neutrino Experiment (DUNE) [26] will also be instrumental in detecting the DSNB in the future. Moreover, the possibility of observing the total—all flavors—DSNB flux via coherent elastic neutrino-nucleus scattering has been recently demonstrated in [27–29]. As a result, the detection of the DSNB in the next few decades will serve as a unique probe of the epoch of neutrino mass generation.

This work is organized as follows. We discuss our modeling of the DSNB flux in Sec. II. We introduce our phenomenological approach to describing mass-varying neutrinos in Sec. III. In Sec. IV, we determine the impact of late neutrino-mass generation on the DSNB fluxes to be measured on Earth. We compute the expected event spectra in a DUNE-like detector in Sec. V. We present our conclusions in Sec. VI. We use natural units where  $\hbar = c = k_{\rm B} = 1$  throughout this manuscript.

#### II. MODELING THE DSNB FLUX

A prediction of the DSNB flux requires a good understanding of the evolution of the Universe, including the rate of core-collapse supernova (CCSN)  $R_{\rm CCSN}$ , as well as a handle on the flavor-dependent neutrino spectra from a SN. The CCSN rate, in turn, depends on the history of the star-formation rate (SFR) and has been measured by a number of independent astronomical surveys [30]. The SFR data can be approximated by the following [31,32]:

$$\dot{\rho}_*(z) = \dot{\rho}_0 \left[ (1+z)^{-10\alpha} + \left( \frac{1+z}{B} \right)^{-10\beta} + \left( \frac{1+z}{C} \right)^{-10\gamma} \right]^{-1/10}, \tag{2.1}$$

where  $\dot{\rho}_0$  is the overall normalization of the rate, and  $\alpha$ ,  $\beta$ , and  $\gamma$  indicate the relevant slopes at different values of z. The parameters B and C are defined as

$$B = (1 + z_1)^{1 - \alpha/\beta},\tag{2.2}$$

$$C = (1 + z_1)^{(\beta - \alpha)/\gamma} (1 + z_2)^{1 - \beta/\gamma}.$$
 (2.3)

We quote the parameters for the SFR used in our work in Table I. A more detailed discussion of these different parameters can be found in [19] and references therein. Using this,  $R_{\rm CCSN}(z)$  can be calculated as

$$R_{\text{CCSN}}(z) = \dot{\rho}_*(z) \frac{\int_8^{100} \psi(M) dM}{\int_0^{100} M \psi(M) dM}, \qquad (2.4)$$

where  $\psi(M) \propto M^{-2.35}$ —the initial mass function (IMF) of stars—gives the density of stars in a given mass range [33]. The lower limit on the IMF indicates tentatively the lowest mass at which a CCSN can form (we neglect lower mass electron capture SNe), while the upper limit is more *ad hoc*, including a reasonable fraction of failed SNe.

Finally, neutrino emission from a SN can be parametrized by the well-known alpha-fit spectra [34]

$$F_{\nu_{\beta}}(E_{\nu}) = \frac{1}{E_{0\beta}} \frac{(1+\alpha)^{1+\alpha}}{\Gamma(1+\alpha)} \left(\frac{E_{\nu}}{E_{0\beta}}\right)^{\alpha} e^{-(1+\alpha)\frac{E_{\nu}}{E_{0\beta}}}, \quad (2.5)$$

where  $E_{0\beta}$  is the average energy for a flavor  $\nu_{\beta}$  or  $\bar{\nu}_{\beta}$ ,  $\beta=e$ ,  $\mu$ ,  $\tau$ , and  $\alpha$  is a parameter that determines the width of the distribution. The DSNB spectra are dominated by neutrino emission from the cooling phase, where the spectra are approximately thermal.  $\alpha=2.3$  approximates Eq. (2.5) as a Fermi-Dirac spectrum [17].

With this information, in the absence of neutrino oscillations, the diffuse neutrino flux from all past SNe is [18,32,35]

$$\Phi_{\nu_{\beta}}^{0}(E) = \int_{0}^{z_{\text{max}}} \frac{dz}{H(z)} R_{\text{CCSN}}(z) \phi_{\nu_{\beta}}^{0}(E(1+z)), \quad (2.6)$$

where  $H(z) = H_0 \sqrt{\Omega_m (1+z)^3 + \Omega_\Lambda}$  is the Hubble function with  $H_0 = 67.36 \text{ km s}^{-1} \text{ Mpc}^{-1}$ , and  $\Omega_m$  and  $\Omega_\Lambda$  represent the matter and vacuum contribution to the energy density, respectively [36]. The integral over z ranges up to the maximum redshift of star formation  $(z_{\text{max}} \sim 5)$ .  $\phi_{\nu_\beta}^0(E)$  in Eq. (2.6), contains contributions from CCSNe and blackhole-forming (BHF) failed SNe,

$$\phi_{\nu_{\beta}}^{0}(E) = f_{\text{CC}}F_{\nu_{\beta}}^{\text{CC}}(E_{\nu}) + f_{\text{BH}}F_{\nu_{\beta}}^{\text{BH}}(E_{\nu}),$$
 (2.7)

where  $f_{\text{CC,BH}}$  are the fraction of CC- and BH-forming explosions, and  $F_{\nu_{\beta}}^{\text{CC,BH}}(E_{\nu})$  are the time-integrated energy spectra for CCSNe and BHF SNe. In the following, we take

TABLE I. Star-formation-rate parameters and their uncertainties used in this work.

Parameter	Value
$\dot{ ho}_0$	$0.0178^{+0.0035}_{-0.0036}~{ m M}_{\odot}~{ m y}^{-1}~{ m Mpc}^{-3}$
$\alpha$	$3.4 \pm 0.2$
β	$-0.3 \pm 0.2$
γ	$-3.5 \pm 1.0$
<i>z</i> <sub>1</sub>	1
$z_2$	4

 $f_{\rm BH}=21$  and  $f_{\rm CC}=1-f_{\rm BH}.$  For the  $F_{
u_{eta}}^{\rm CC,BH}(E_{
u}),$  we have performed a fit of the time-integrated neutrino fluences obtained by the Garching group [37] in the form of Eq. (2.5), taking as benchmark the data for 12  $M_{\odot}$  for CCSNe and 40  $M_{\odot}$  as for BHF SNe. For the stars undergoing collapse into a BH, neutrino emission exists until the point of BH collapse. On the other hand, for the corecollapse SN, we have considered the time evolution up to the maximum time  $[\sim \mathcal{O}(1)]$  s as provided in the simulations. We have also checked by considering a few different models of solar mass for both the cases and found the resultant DSNB spectra to be qualitatively similar. We present in Fig. 1 the unoscillated fluxes at Earth, obtained from Eq. (2.6) for  $\nu_e$  (orange),  $\bar{\nu}_e$  (green dashed), and  $\nu_x = \nu_u, \nu_\tau, \bar{\nu}_u, \bar{\nu}_\tau$ , and the corresponding antineutrinos (purple dotted). The  $\nu_e$  flux is about twice the  $\nu_x$  flux at  $E \sim 3.5$  MeV. The bands correspond to the uncertainty related to the star-formation rate. Let us notice that there are

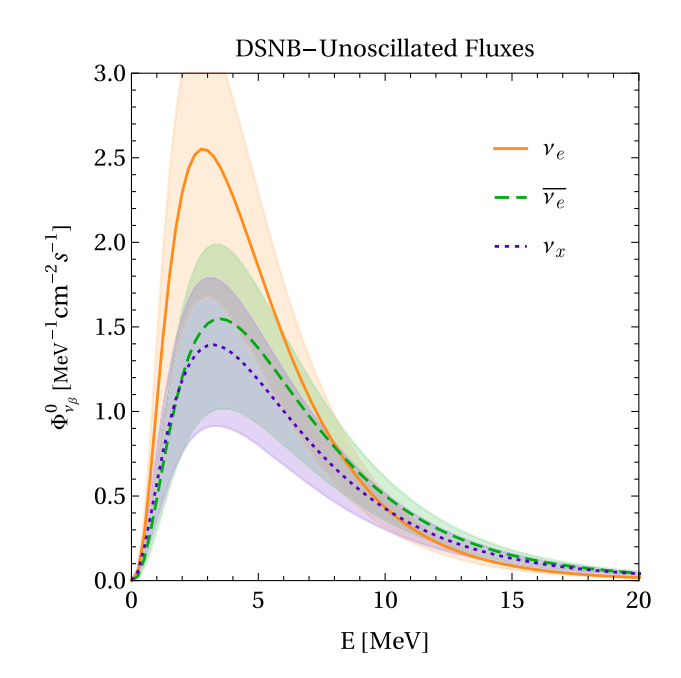


FIG. 1. Unoscillated DSNB flux  $\Phi^0_{\nu_\beta}$  for each neutrino species,  $\nu_e$  (orange),  $\bar{\nu}_e$  (green dashed), and  $\nu_x$  (purple dotted) as a function of the neutrino energy E. The bands are associated with uncertainties in the star-formation rate.

other sources of uncertainty, such as the actual value of the BH-forming fraction, spectral shape, etc., see Ref. [38] for a detailed review of the uncertainties affecting the DSNB. This difference arises mainly due to the interactions with neutrons that render the average energy of the  $\nu_e$  flux smaller. Meanwhile, the  $\bar{\nu}_e$  and  $\nu_x$  have closer average energies, making the fluxes much more similar. Such difference will be crucial in our scenario of mass-varying neutrinos.

The neutrino flux gets processed through oscillation effects inside the SN and on the way to Earth. In this study, we neglect the effects of collective neutrino oscillations arising out of neutrino self-interactions deep inside the SN [39,40]. The quantitative impact of collective oscillations is inconclusive to date, and we expect it to be relatively smaller for neutrinos predominantly produced in the cooling phase. The neutrino flux gets affected by adiabatic Mikheyev-Smirnov-Wolfenstein (MSW) resonant flavor conversion [41]. Assuming NO, this implies that the  $\nu_e$  are primarily emitted as  $\nu_3$ , while the nonelectron neutrinos  $\nu_{\mu,\tau}$  are emitted as combinations of  $\nu_1$  and  $\nu_2$ . In this case, the final  $\nu_e$  flux at Earth  $\Phi_{\nu_e}(E)$  is given by

$$\Phi_{\nu_e}(E) = |U_{e3}|^2 \Phi_{\nu_e}^0 + (1 - |U_{e3}|^2) \Phi_{\nu_x}^0, \qquad (2.8)$$

where  $\Phi^0_{\nu_x} = \Phi^0_{\nu_\mu} = \Phi^0_{\nu_\tau}$ , and  $U_{\alpha i}$  is the Pontecorvo-Maki-Nakagawa-Sakata (PMNS) mixing matrix. Clearly, the DSNB flux depends on the underlying neutrino oscillation scenario. For example, if the neutrinos were massless at the time of the SN, the flavor evolution of the  $\nu_e$  and  $\nu_x$  (and the antineutrinos) would be trivial inside the explosion. On their way here, these would start oscillating, fast, once the neutrino masses turn on. In this case, the probability that a  $\nu_\alpha$  is detected as a  $\nu_e$  at Earth is

$$P_{\alpha e} = \sum_{i} |U_{\alpha i}|^2 |U_{e i}|^2. \tag{2.9}$$

Since SN neutrino energies are smaller than the muon mass, it is convenient to define  $P_{xe} = P_{\mu e} + P_{\tau e} = 1 - P_{ee}$  so

$$\Phi_{\nu_{\sigma}}(E) = P_{ee}\Phi_{\nu_{\sigma}}^{0} + (1 - P_{ee})\Phi_{\nu_{\sigma}}^{0}. \tag{2.10}$$

In the next sections, we discuss in detail how the DSNB is modified if a fraction of it comes from neutrinos that were "born" with smaller masses or different mixing parameters.

# III. MASS-VARYING NEUTRINOS

Following [13,14,42], we assume that the neutrinos remain practically massless down to a certain redshift  $z_s$  and gain a nonzero mass for  $z < z_s$ . We further assume the neutrino mass reaches its current value over a finite transition period. This could happen due to neutrinos coupling to the gravitational- $\theta$  term, causing a late phase transition in the Universe [14], or to neutrinos coupled to a

scalar background, which evolves as a function of time [10–12,43]. Here, we remain agnostic regarding the details of mass generation.

Assuming momentarily there is only one neutrino mass, we propose that it varies as a function of redshift according to

$$m_{\nu}(z) = \frac{m_{\nu}}{1 + (z/z_s)^{\mathrm{B}_s}},$$
 (3.1)

where  $m_{\nu}$  is the current mass of the neutrino,  $B_s$  is a parameter that controls the width of the transition from a massless neutrino to a massive neutrino, and  $z_s$  is the redshift below which the neutrino mass turns on. The specific form of the function is irrelevant and is chosen just to present a smooth transition to a nonzero mass. The values of  $z_s$  and  $B_s$  determine when and at what rate the neutrino mass turns on.

Since there are three neutrino masses, it is possible that they would "turn on" at different  $z_s$  and that the transition would be associated with a different value of  $B_s$ . Here we assume a universal value for these two phenomenological parameters. It is also possible to imagine that, as the neutrino mass turns on at  $z_s$ , so do all the PMNS mixing angles  $\{\theta_{12}, \theta_{13}, \theta_{23}\}$ , and that these turn on in a way that is also captured by Eq. (3.1). We will discuss this possibility later but remain agnostic about the origin of such variations.

In the next section, we will detail the impact of redshiftdependent neutrino masses and mixing angles on the flavor evolution of neutrinos within the SN, as well as from the SN to Earth.

# IV. IMPACT OF MASS-VARYING NEUTRINOS ON THE DSNB

### A. Only masses

We first consider the case where the neutrino masses vary as a function of red-shift, while the elements of the mixing matrix are time independent.

# 1. Calculation of the survival probability

In the standard three-massive-neutrinos paradigm, neutrinos produced via charged-current weak interactions are described as superpositions of the three neutrinos with well-defined masses,  $\nu_{\alpha}=U_{\alpha i}\nu_{i},~\alpha=e,~\mu,~\tau,~i=1,~2,~3.$  During propagation, the fact that the neutrino masses are different leads the neutrino flavor to oscillate; the associated oscillation lengths are inversely proportional to the differences of the squares of the neutrino masses. Global analysis of the present data indicate that the two independent mass-squared differences are  $\Delta m_{21}^2 \sim 7.5 \times 10^{-5}$  and  $\Delta m_{31}^2 \sim \pm 2.5 \times 10^{-3} \text{ eV}^2$  (plus for NO, minus for IO) [4]. In matter, the neutrino flavor evolution is modified by the forward elastic neutrino-electron interaction amplitude

along the neutrino path.<sup>1</sup> This interaction is captured by a matter potential and modifies the effective Hamiltonian that describes neutrino flavor evolution [44,45]. The matter potential depends on the electron number density  $(n_e)$  along the neutrino path. For position-dependent matter potentials, flavor evolution is rather involved. For certain matter profiles, however, the phenomenon is well understood [46–50]. The case where neutrinos are produced in a region of space where  $n_e$  is large and propagate toward the direction where  $n_e$  falls roughly exponentially is well known and applies to both solar neutrinos and neutrinos produced in the core of SN explosions.

In the limit where  $G_F n_e$ , where  $G_F$  is the Fermi constant, is much larger than  $|\Delta m^2/E|$ , where E is the neutrino energy and  $\Delta m^2$  are the neutrino-mass-squared differences, electron neutrinos coincide with one of the propagation-Hamiltonian eigenstates (the one with the largest eigenvalue) in the production region. If neutrino flavor evolution is adiabatic inside the medium, the electron neutrino exits the matter distribution as a mass eigenstate (eigenstate of the flavor-evolution Hamiltonian in vacuum). This "mapping" between the electron neutrino and mass eigenstates depends on the mass ordering and whether we are considering electron neutrinos or antineutrinos, keeping in mind that the matter potential is positive for neutrinos and negative for antineutrinos.

Given what we know about the mass-squared differences, electron neutrinos, if the flavor evolution inside the SN is adiabatic, exit the SN as  $\nu_3$  for NO and  $\nu_2$  for IO. Electron antineutrinos, instead, exit the SN as  $\bar{\nu}_1$  for NO and  $\bar{\nu}_3$  for IO. In the adiabatic regime, it is easy to generalize this picture to the case where  $G_F n_e$  is not much larger than one or both  $\Delta m^2/E$ : the flavor evolution along the matter potential is just described by the effective mixing parameters at neutrino production. In the case of two neutrino flavors, if the electron number density decreases roughly exponentially, adiabaticity is controlled by the "crossing probability"  $P_c$ . When  $P_c$  vanishes, the flavor evolution is perfectly adiabatic.  $P_c$  is given by [47–49]

$$P_{c} = \frac{\exp^{-(\pi\gamma F/2)} - \exp^{-(\pi\gamma F/2\sin^{2}\theta)}}{1 - \exp^{-(\pi\gamma F/2\sin^{2}\theta)}},$$
 (4.1)

where F depends on the matter distribution inside the supernova and the mixing angle [51]. The dependence of  $P_c$  on the oscillation parameters  $\Delta m^2$  and  $\theta$  is controlled by  $\gamma$ , which takes the following expression around the resonant region, defined by  $n_e$  values that satisfy  $2\sqrt{2}G_FEn_e = \Delta m^2\cos 2\theta$ :

$$\gamma = \frac{\Delta m^2}{2E} \frac{\sin^2 \theta}{\cos 2\theta} \left( \frac{1}{n_e} \frac{dn_e}{dr} \right)^{-1}.$$
 (4.2)

If the variation of the effective mixing angles with the electron number density is slower than the oscillation wavelength in matter,  $\gamma F \gg 1$  and the neutrino evolution is adiabatic.

It is easy to generalize the discussion to three flavors, taking advantage of the fact that the magnitudes of the two known mass-squared differences differ by 2 orders of magnitude. In this case, one can define two resonance regions and two crossing probabilities:  $P_c^H$  (H for high), associated with  $\Delta m^2 = \Delta m_{31}^2$  and  $\theta = \theta_{13}$ , and  $P_c^L$  (L for low), associated with  $\Delta m^2 = \Delta m_{21}^2$  and  $\theta = \theta_{12}$ . In our computations, in the standard case and NO, we use, for  $P_c^H$ ,  $\Delta m_{31}^2 = 2.57 \times 10^{-3} \text{ eV}^2$  and  $\theta_{13} = 8.57^\circ$  and, for  $P_c^L$ ,  $\Delta m_{21}^2 = 7.42 \times 10^{-5} \text{ eV}^2$  and  $\theta_{12} = 33.44^\circ$  [4].

The flavor-at-production and the neutrino spectrum emitted by the supernova depends on the evolution of the collapse of the star. After the shock wave, free electrons are captured by free protons generated by the dissociation of nuclei yielding a  $\nu_e$ -rich flux—the neutronization burst. Thereafter, a large fraction of the neutrinos are emitted during the cooling phase when the supernova loses the remaining gravitation binding energy via the thermal emission of neutrinos of all flavors. In this phase, the temperature of  $\nu_e$  is expected to be smaller than that of  $\bar{\nu}_e$  and that of  $\nu_x$ , since  $\nu_e$  interacts more strongly with the production medium.

Most of the neutrinos are created deep inside the explosion where the density is quite large. The neutrino spectra depend negligibly on the neutrino masses. In fact, in hydrodynamic CCSN simulations, the neutrinos are treated as massless classical particles. So, we do not expect the neutrino spectra to depend on the origin of the neutrino mass. The only place where neutrino mass plays a role is in deciding the difference between mass and flavor eigenstates.

On their way out, neutrinos cross both the atmospheric  $(\rho \sim 3 \times 10^3 \text{ g/cm}^3)$  and the solar resonances  $(\rho \sim 40 \text{ g/s})$ cm<sup>3</sup>) at lower densities. Both resonances happen well outside of the neutrinospheres. In Fig. 2, we depict contours of constant  $P_c$  in the  $\Delta m^2 \times \sin^2 2\theta$  plane. We identify three qualitatively distinct regions: (I)  $P_c < 0.1$ , where flavor evolution "through" the resonance is adiabatic, (II) 0.1 < Pc < 0.9, and (III)  $P_c > 0.9$ , where neutrino flavor evolution is highly nonadiabatic. Given the current values of the mass-squared differences (z = 0 in the figure), flavor evolution is very adiabatic through both the atmospheric and solar resonances [52]. The large value of the density in the region where the neutrinos are produced leads to, as discussed earlier,  $\nu_e$  being mapped to the most massive state (e.g.,  $\nu_3$  for NO), while the  $\nu_x$  is mapped into the lighter states (e.g., for NO, some combination of  $\nu_1$  and  $\nu_2$ ). In this case, for NO, the flux of electron neutrinos at Earth is given by the projection of the three massive states weighted by the

<sup>&</sup>lt;sup>1</sup>As mentioned earlier, we will ignore collective effects throughout.

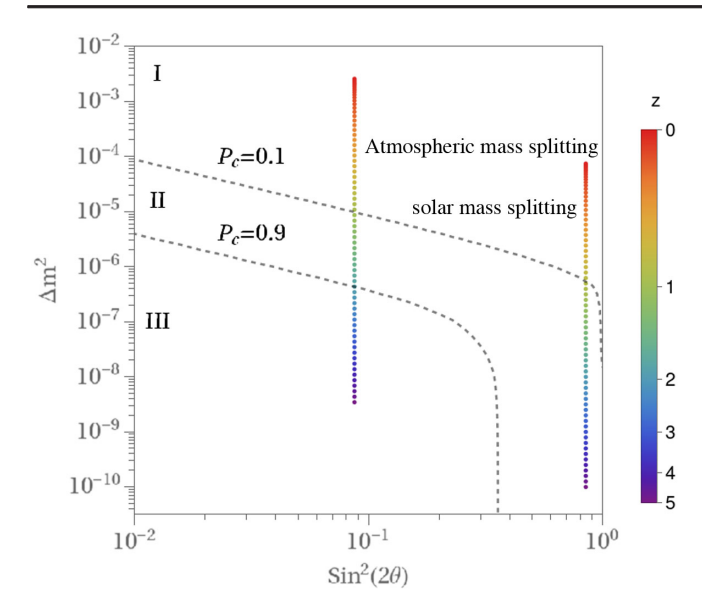


FIG. 2. Constant crossing probability contours in the  $\sin^2 2\theta \times \Delta m^2$  plane. These define three regions: (I)  $P_c < 0.1$ , (II)  $0.1 < P_c < 0.9$ , and (III)  $P_c > 0.9$ . The color scale indicates the values of the two independent mass-squared differences as a function of the redshift of neutrino production. For the mass variation, we make use of Eq. (3.1) with  $z_s = 0.32$  and  $B_s = 5$ .

initial flux, Eq. (2.8). The small value of  $|U_{e3}|^2 \sim 0.02$  implies that most of the  $\nu_e$  at Earth started out as a  $\nu_x$  deep inside the explosion. Note that we have not considered the effects of propagation through a shock wave in our study, as this can introduce additional nonadiabaticity in the flavor propagation. This will make it difficult to disentangle the effects of propagation through a shock wave from that of switching on a nonzero neutrino mass. We have considered a SN matter profile characteristic of the cooling phase, where the effects of the shock wave are less distinct. Since the DSNB are time-integrated spectra, we expect the effects from the cooling phase matter profile to be the most dominant. Effects due to nonadiabaticity introduced due to the shock wave propagation or additional turbulence due to a reverse shock will be negligible.

If the neutrino masses were smaller at a given time in the history of the Universe, the flavor evolution inside the supernova might no longer be adiabatic. This is depicted in Fig. 2, where we indicate the different values of the mass-squared differences for different redshifts, following Eq. (3.1) with  $z_s = 0.32$  and  $B_s = 5$ . This allows for the possibility that one massive state "flips" into another one as the neutrinos propagate through the supernova. In the case of a nonadiabatic evolution and NO, the initial  $\nu_e$  component of the flux will also be partially mapped to  $\nu_1$  and  $\nu_2$  fluxes outside the SN. Following [52], the  $\nu_e$  flux at Earth in the case of a nonadiabatic evolution is given by Eq. (2.10), where the  $\nu_e$  survival probability  $P_{ee}$  is given by

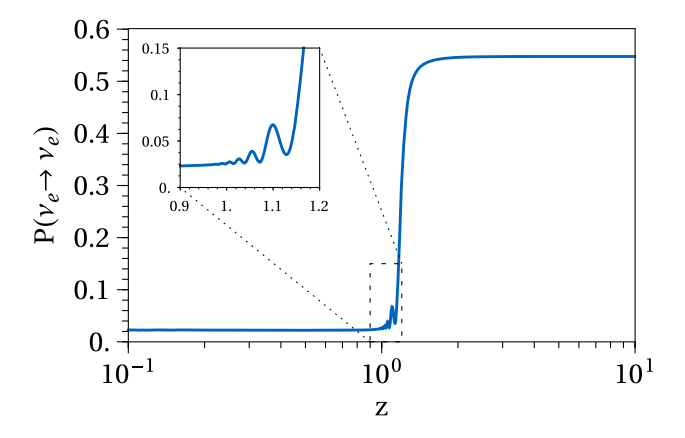


FIG. 3. Electron-neutrino survival probability as function of the redshift for  $E_{\nu}=10$  MeV. We consider that the mass changes as a function of the redshift according to Eq. (3.1) for  $z_s=0.32$  and  $B_s=5$ .

$$\begin{split} P_{ee} = & |U_{e1}|^2 P_c^H P_c^L + |U_{e2}|^2 (P_c^H - P_c^H P_c^L) + |U_{e3}|^2 (1 - P_c^H). \end{split} \tag{4.3}$$

In the adiabatic limit ( $P_c^L = P_c^H = 0$ ), we recover the standard expression for the  $\nu_e$  flux at Earth, Eq. (2.8). As the neutrino masses decrease, the atmospheric and solar resonances shift to lower densities. Note that, if the neutrino mass is low enough, the neutrinos might not "cross" one of the resonances on their way out of the SN. That will also impact the final  $\nu_e$  flux.

In the case of the normal mass ordering, the nonadiabatic evolution leads to an enhancement of the  $\nu_e$  flux because the initial  $\nu_e$  flux is larger than that of the other flavors. Figure 3 depicts the electron-neutrino survival probability on Earth as a function of the redshift z of the SN, for  $E_{\nu}=10$  MeV,  $z_s=0.32$ , and  $B_s=5$ . For this choice of mass-varying parameters, the transition between massless and massive neutrinos happens around  $z\sim1$ . If the neutrino energy increases, the transition shifts to lower redshifts. Around  $z\sim1$ , we observe a small oscillatory pattern in  $P_{ee}$ , highlighted in the inset. For those values of z,  $\Delta m_{21}^2\sim10^{-8}$  eV<sup>2</sup> and the associated oscillation length is on order of the size of the SN.

# 2. The DSNB $\nu_e$ flux on Earth

In order to include the possibility that neutrino masses are redshift dependent, Eq. (2.8) needs to be altered,

$$\Phi_{\nu_e}(E) = \int_0^{z_{\text{max}}} \frac{dz}{H(z)} R_{\text{CCSN}}(z) \{ P_{ee}(z) \phi_{\nu_e}^0 + (1 - P_{ee}(z)) \phi_{\nu_e}^0 \},$$
(4.4a)

$$\begin{split} \Phi_{\tilde{\nu}_e}(E) &= \int_0^{z_{\text{max}}} \frac{dz}{H(z)} R_{\text{CCSN}}(z) \{ \overline{P_{ee}}(z) \phi_{\tilde{\nu}_e}^0 \\ &+ (1 - \overline{P_{ee}}(z)) \phi_{\nu_x}^0 \}, \end{split} \tag{4.4b}$$

$$\begin{split} \Phi_{\nu_{x}}(E) &= \int_{0}^{z_{\text{max}}} \frac{dz}{H(z)} R_{\text{CCSN}}(z) \frac{1}{4} \{ (1 - P_{ee}(z)) \phi_{\nu_{e}}^{0} \\ &+ (1 - \overline{P_{ee}}(z)) \phi_{\bar{\nu}_{e}}^{0} + (2 + P_{ee}(z) + \overline{P_{ee}}(z)) \phi_{\nu_{x}}^{0} \}, \end{split}$$
 (4.4c)

where, for clarity, we omitted the dependence of  $\phi^0_{\nu_\beta}$  on (E,z).  $P_{ee}(z)$  [ $\overline{P}_{ee}(z)$ ] indicate the oscillation probabilities for neutrinos (antineutrinos) from a SN explosion at a redshift z as described in the last subsection. It depends on the  $B_s$ ,  $z_s$  parameters, so the final DSNB flux will contain information regarding them. The DSNB is an integrated flux, so, in principle, there is no explicit way to distinguish neutrinos that were emitted at higher redshifts from those produced more recently. However, the energies of the neutrinos produced earlier are more redshifted, and hence we expect that time-dependent neutrino masses will distort the DSNB energy spectrum.

We first consider the case where only the neutrino masses change over time, assuming the NO. Figure 4, left, depicts the electron-neutrino flux at Earth for different values of  $z_s \in [10^{-2}, 1]$ , for  $B_s = 5$ . The standard flux for constant neutrino masses, including uncertainties associated with the SFR, is depicted as the orange band, while the dashed orange line corresponds to the unoscillated DSNB flux  $\Phi^0_{\nu_e}$  (i.e., expectations in the scenario where all neutrino masses are exactly zero). We observe that the hypothesis that neutrino masses depend on the redshift can significantly impact the DSNB electron-neutrino flux for

 $z_s \lesssim 0.5$ . In fact, for E = 3 MeV, the DSNB flux can be larger than standard expectations by a factor on order of 1.4 for  $z_s \sim 10^{-2}$ . Moreover, from a simple flux conservation argument, this also implies that the flux at larger energies is reduced with respect to the standard case; see the inset plot. Such neutrinos would have acquired their masses rather recently, when the Universe was 13.652 Gyr old (compare with the age of the Universe  $t_0 = 13.795$  Gyr), therefore the DSNB was mostly produced when neutrinos were virtually massless. The increment on the  $\nu_e$  flux at low energies is directly related to the difference between the unoscillated  $\nu_e$  and  $\nu_x$  fluxes. In the standard scenario  $P_{ee} \ll 1$ , so the  $\nu_e$  flux at Earth is basically the  $\nu_x$  flux produced at the neutrinosphere, which is much broader in energy. However, if  $P_{ee}$  significantly differs from the standard case, the contribution from the  $\nu_e$  flux that exited the neutrinosphere becomes significant, thus modifying the  $\nu_e$  flux at Earth.

For values of  $0.1 \lesssim z_s \lesssim 1$ , the  $\nu_e$  flux is still larger than the SM flux at low energies. Meanwhile, for  $z_s \gtrsim 1$ , the DSNB flux is basically indistinguishable from the standard case. To understand the dependence on the values of  $z_s$ , we show in the right panel of Fig. 4 the redshift evolution of neutrino masses along with the factor  $R_{\rm CCSN}(z)/H(z)$ , cf. Eq. (2.6). This object describes the SN neutrino production as a function of redshift, including effects associated with the expansion of the Universe. It reveals that most of the DSNB flux is produced at  $0.1 \lesssim z \lesssim 5$ . Thus, if  $z_s \gtrsim 1$ , the SN matter effects are basically the same as in the standard case, so we do not expect any impact

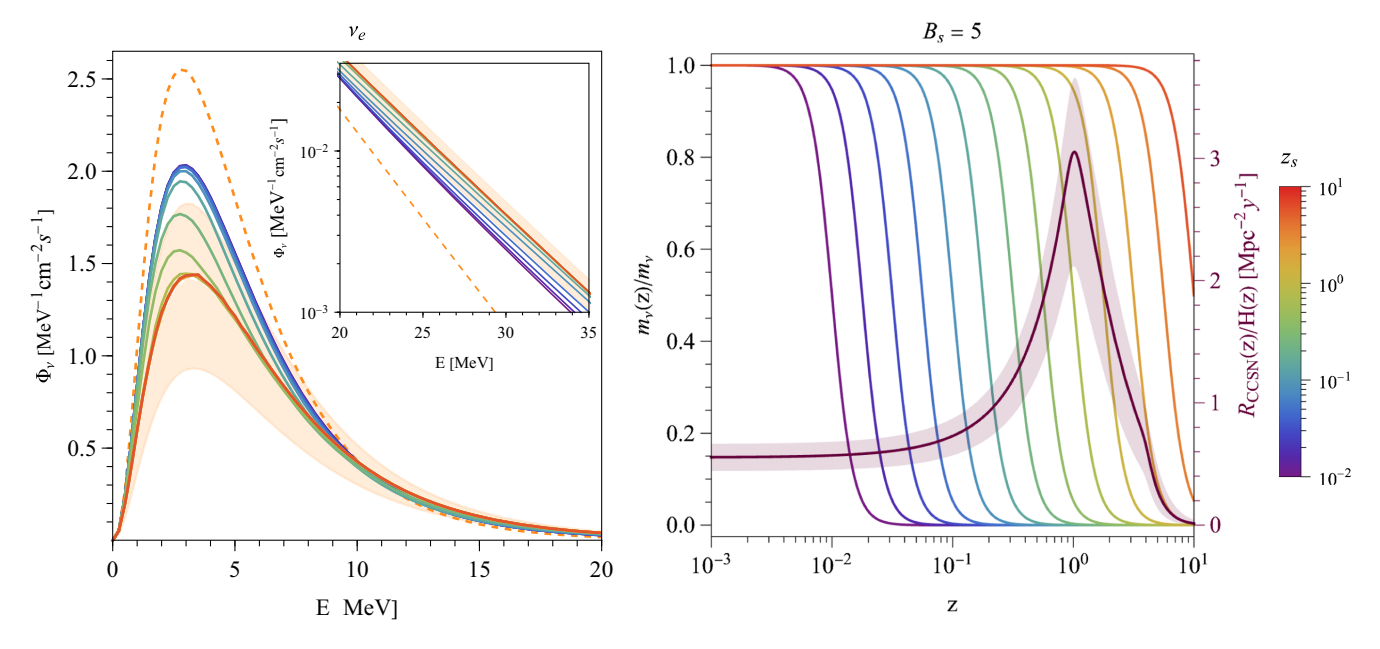


FIG. 4. Left: the DSNB  $\nu_e$  flux as a function of the neutrino energy for different values of  $z_s \in [10^{-2}, 1]$  (rainbow colored) and for the standard case (orange) including the star-formation-rate uncertainty (orange band). The dashed orange line indicates the DSNB flux assuming massless neutrinos, i.e.,  $P_{ee}(z) = 1$  for all z. Right: neutrino mass as a function of redshift z, normalized to the current value of the mass,  $m_{\nu}(z)/m_{\nu}$ , together with  $R_{\rm CCSN}(z)/H(z)$ . See text for details. On both sides of the figure,  $B_s = 5$ . We assume the normal ordering for the neutrino masses.

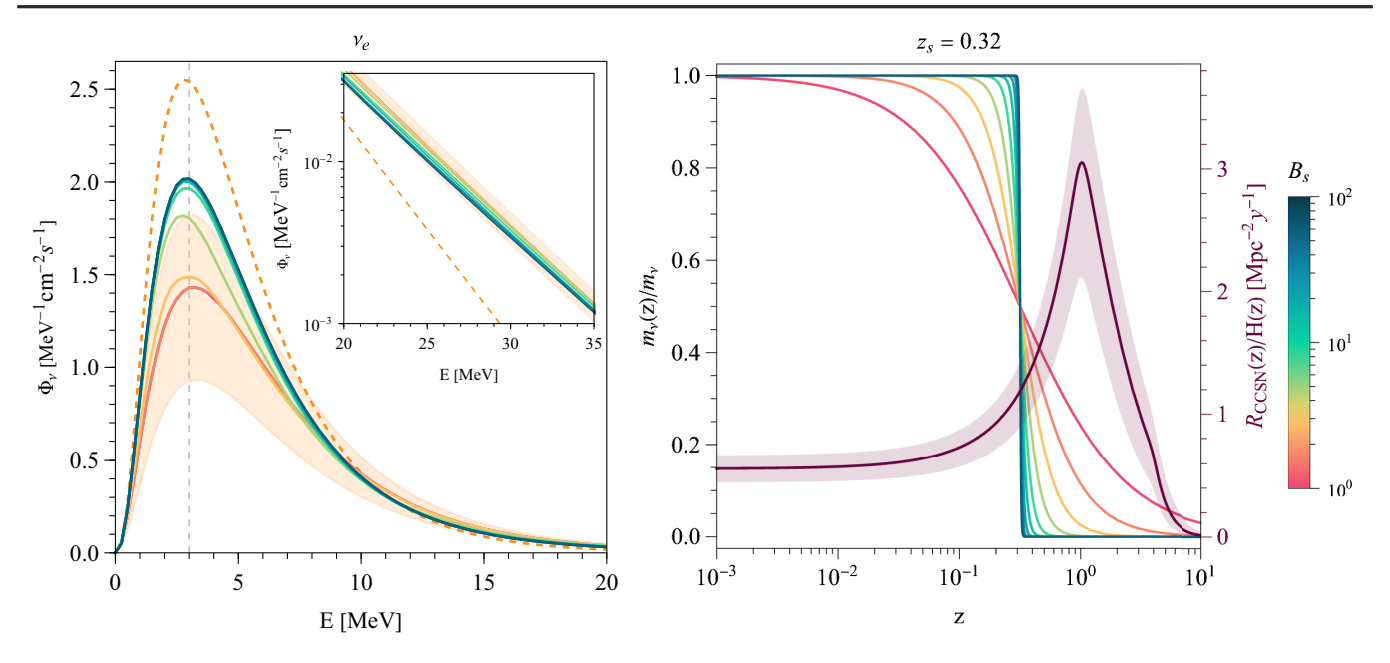


FIG. 5. Same as Fig. 4, for different values of  $B_s \in [1, 100]$  and fixed  $z_s = 0.32$ .

from the mass-varying hypothesis. On the other hand, if  $0.1 \lesssim z_s \lesssim 1$ , a significant fraction of the DSNB comes from SN explosions that happened when the neutrino masses were significantly smaller. The largest effects occur when neutrinos were effectively massless during most of the history of the Universe,  $z_s \lesssim 0.1$ , as noted above.

Figure 5 captures the dependence of the DSNB flux on the parameter  $B_s$  for a fixed  $z_s = 0.32$ .  $B_s$  controls how fast neutrino masses increase, larger values being associated with more abrupt transitions. For  $B_s \gtrsim 10$ , the transition is almost instantaneous. Whenever the growth of neutrino masses is rapid (B<sub>s</sub>  $\gtrsim$  50), the flux is relatively larger (by the same factor, discussed earlier,  $\Phi_{\nu_e}/\Phi_{\nu_e}|_{\rm SM}\sim 1.4$ ). This dependence on B<sub>s</sub> again is understood by comparing the redshift dependence of both  $m_{\nu}(z)$  and  $R_{\rm CCSN}(z)/H(z)$ (right panel). If the masses become nonzero instantaneously, neutrinos emitted before the transition  $(z > z_s)$ would have been effectively massless, and their contribution to the  $\nu_e$  flux will be associated with the electronneutrino survival probability  $P_{ee} = \sum_{k} |U_{ek}|^4 \approx 0.57$ , characteristic of electron neutrinos propagating very long distances in vacuum. After the masses turn on, neutrinos will be subject to matter effects inside the SN and  $P_{ee}$  =  $|U_{e3}|^2$  in the NO, as discussed earlier. The final DSNB flux will be an amalgam of neutrinos from two different epochs whose contributions are weighted by the SFR divided by the expansion rate. If the transition is not instantaneous (small B<sub>s</sub>), the DSNB flux is reduced because matter effects would impact the propagation inside the SN for a longer period of time and the neutrino masses would be on the order of the current masses for an extended range of redshifts (when the neutrino masses are \$\ge 10\% of the masses today, the matter effects are very similar to the standard case). Thence, the DSNB flux in such cases is closer to the standard case, as can be observed in Fig. 5.

So far, we have focused on the impact of redshiftdependent neutrino masses on the  $\nu_e$  flux assuming NO. Instead, the impact on the  $\bar{\nu}_e$  spectrum is minimal. This is depicted in Fig. 6, left, for NO. This indifference is not strongly dependent on the mass ordering and is mostly a consequence of the fact that the original  $\bar{\nu}_e$  and  $\nu_x$  fluxes (keeping in mind that  $\nu_x$  includes the antineutrino flavors) are very similar, see Fig. 1. In this case, oscillation effects are invisible. Nonetheless, it is worth discussing the oscillation of  $\bar{\nu}_e$  in a little more detail. The standard prediction assuming adiabatic propagation indicates that  $\bar{\nu}_e$  emerges from the SN as  $\bar{\nu}_1$  so  $\overline{P_{ee}} = |U_{e1}|^2 \approx 0.67$  at low energies. The  $\bar{\nu}_e$  flux at Earth is, therefore, roughly an equal admixture of  $\Phi^0_{ar{
u}_{\scriptscriptstyle F}}$  and  $\Phi^0_{
u_{\scriptscriptstyle X}}$ , fluxes that are close to each other. Furthermore, if neutrino masses arise later in the evolution of the Universe ( $z_s \lesssim 0.1$ ),  $\overline{P_{ee}} \sim 0.57$  as in the  $\nu_e$ case. The difference between these fluxes is safely within the star-formation-rate uncertainty, making the effect unobservable, even in the most optimistic cases. Similarly,  $\nu_x$ , measurable only via neutral current interactions at these low energies, is also modified in a negligible way, as can be observed in the right panel of Fig. 6 for NO. Since it contains the contributions of both neutrinos and antineutrinos, the modification of this flux is at most 10%, within the star-formation-rate uncertainty.

For the IO, the situation changes significantly for  $\nu_e$ . In the standard scenario, the MSW effect predicts that the  $\nu_e$  created at the neutrinosphere leaves the SNe as a  $\nu_2$  mass eigenstate, so  $P_{ee} = |U_{e2}|^2 \sim 0.3$ . Meanwhile, if neutrinos only acquired their masses recently  $(z_s \lesssim 1)$ , we would have the same probability as in the NO,

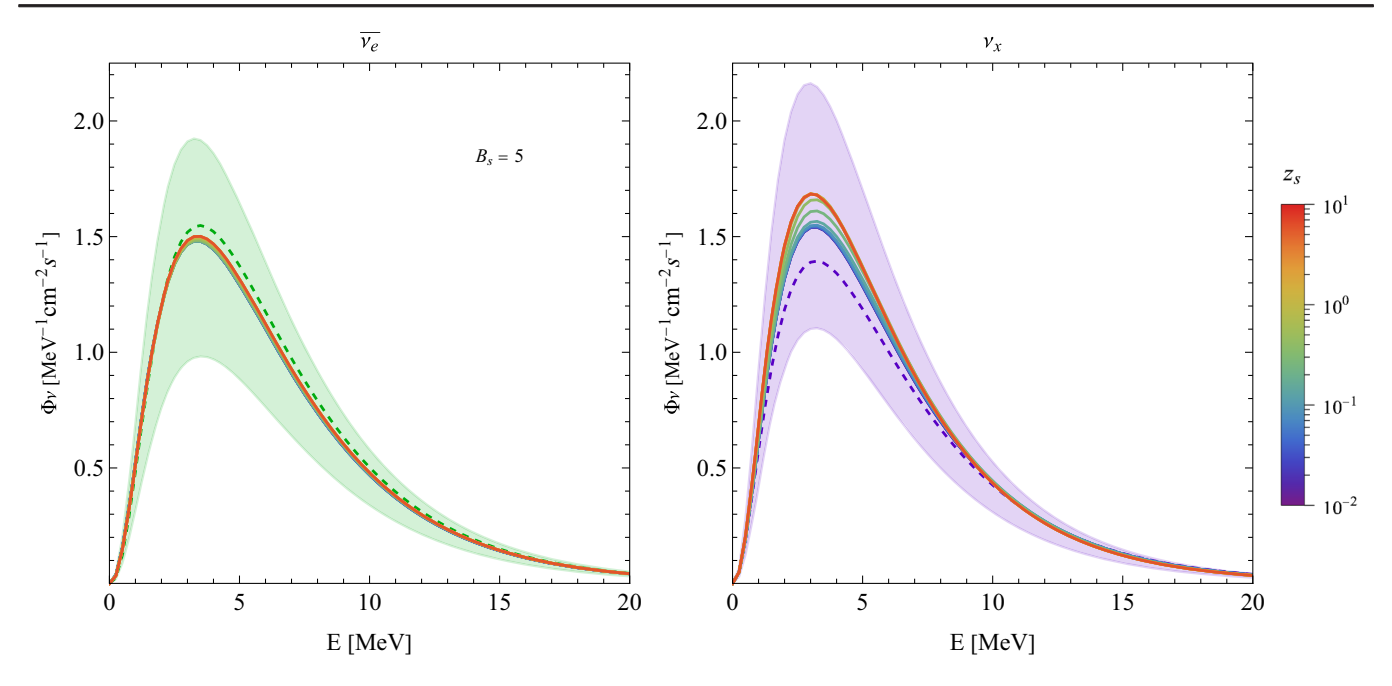


FIG. 6. The DSNB  $\bar{\nu}_e$  flux (left) and  $\nu_x$  flux (right) as a function of the neutrino energy for different values of  $z_s \in [10^{-2}, 1]$  (rainbow colored) and fixed  $B_s = 5$ . The fluxes in the standard case, including the star-formation-rate uncertainty, define the green (left) and purple (right) bands. The dashed lines indicate the DSNB flux assuming massless neutrinos. We assume the normal ordering for the neutrino masses.

 $P_{ee} = \sum_k |U_{ek}|^4 \approx 0.57$ . Thus, we find that any possible modification on the DSNB energy spectrum in the IO will lie within the current star-formation uncertainty band. On the other hand, for antineutrinos and the IO, we have  $\overline{P_{ee}} = |U_{e3}|^2$ , so, if matter effects inside the SNe were significantly different at some point of the evolution of the Universe,  $\overline{P_{ee}}$  would be considerably different from the standard value. Nevertheless, since  $\Phi^0_{\nu_x}$  and  $\Phi^0_{\overline{\nu}_e}$  are very similar, cf. Fig. 1, any imprint of the mass-varying hypothesis would be very difficult to measure.

#### B. Masses and mixing

If one allows for the possibility that the neutrino masses are redshift dependent, it is reasonable to ask whether the neutrino mixing parameters also depend on the redshift. We address this possibility in this subsection.

# 1. Calculation of the survival probability

In the case where both the neutrino masses and the mixing parameters depend on the redshift, the adiabaticity of the neutrino flavor evolution inside the SN is modified relative to the case where only the masses depend on the redshift. Similar to Fig. 2, Fig. 7 depicts contours of constant  $P_c$  in the  $\Delta m^2 \times \sin^2 2\theta$  plane along with the z-dependent values of the oscillation parameters. Here, however, both the masses and mixing angles go to zero as z grows. Explicitly, we postulate that the redshift-dependent mixing angles  $\theta_{ij}$ , ij = 12, 13, 23 are

$$\theta_{ij}(z) = \frac{\theta_{ij}}{1 + (z/z_s)^{\mathbf{B}_s}}. (4.5)$$

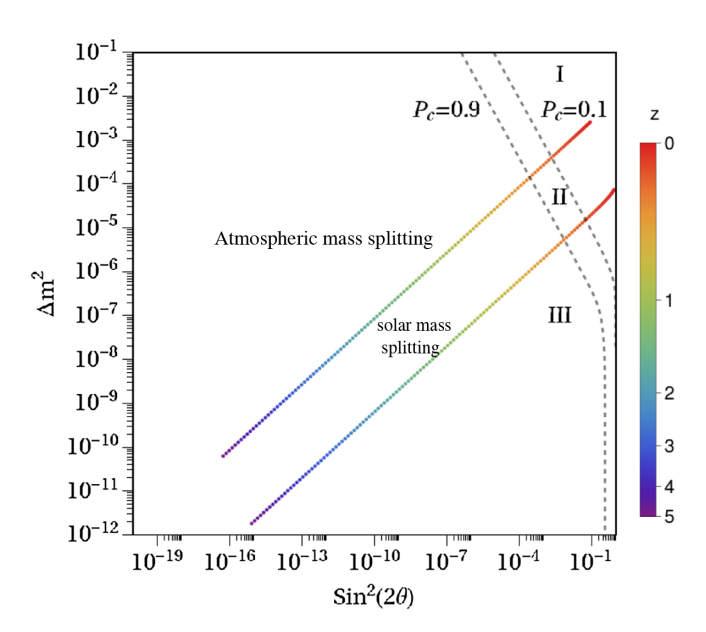


FIG. 7. Constant crossing probability contours in the  $\sin^2 2\theta \times \Delta m^2$  plane. These define three regions: (I)  $P_c < 0.1$ , (II)  $0.1 < P_c < 0.9$ , and (III)  $P_c > 0.9$ . The color scale indicates the values of the two independent sets of oscillation parameters  $-\Delta m_{31}^2$  and  $\sin^2 2\theta_{13}$  (Atm) and  $\Delta m_{21}^2$  and  $\sin^2 2\theta_{12}$  (Sol)—as a function of the redshift of neutrino production. For the mass variation, we make use of Eq. (3.1) with  $z_s = 0.32$  and  $B_s = 5$ .

Similar to the mass-varying scenario, the nonadiabatic evolution of the neutrinos for smaller masses and mixing angles will lead to an enhancement of the  $\nu_e$  flux at Earth. The lower values of the mixing parameters imply that the flavor resonances happen at lower electron number densities. The minimum densities considered here are around 2 g/cm<sup>3</sup>. If the MSW resonance happens at lower densities, neutrinos will not cross them as they exit the supernova. In this case, flavor evolution resembles the vacuum case [53]. For  $B_s = 5$  and  $z_s = 0.32$ , this happens for  $z \sim 1.3$  for the "atmospheric" resonance and  $z \sim 0.6$  for the solar one.

# 2. The DSNB $\nu_e$ flux at Earth

We compute the DSNB flux as discussed around Eq. (4.4a), this time including in the z dependency of  $\theta_{ij}(z)$  ( $ij = \{12, 13, 23\}$ ). As in the previous subsection, we concentrate on the NO and on electron neutrinos, where we anticipate the strongest effects. Similar to the results presented in the last subsection, Fig. 8 depicts the DSNB  $\nu_e$  flux as function of the neutrino energy for different values of  $z_s$  and  $B_s$ . In the left panel, we fix  $B_s = 5$  and vary  $z_s \in [10^{-2}, 10]$ . In the right panel, we fix  $z_s = 0.3$  and vary  $B_s \in [1, 100]$ . We observe that the enhancement of  $\Phi_{\nu_e}/\Phi_{\nu_e}|_{\rm SM} \sim 1.5$  at E = 3 MeV is larger than what we found in the mass-only varying case. At higher energies, instead, the flux is relatively suppressed by a factor ranging from roughly 0.6 for E = 20 MeV to 0.4 at E = 50 MeV. Hence, the fact that the mixing angles also decrease with

increasing redshift leads to more pronounced effects. Taking as example  $z_s = 0.05$ ,  $B_s = 5$ , we find that a  $\nu_e$  emitted at redshifts  $z \gtrsim z_s$  will exit mostly as a  $\nu_1$  (assuming the normal mass ordering) since the mixing angles are small enough that the PMNS matrix is effectively diagonal. After exiting the supernova, neutrino masses turn on in such a way that they remain a  $\nu_1$  throughout. Thus, at Earth, the electron survival probability is simply  $P_{ee} = |U_{e1}|^2 \approx 0.67$ , which enhances the observable  $\nu_e$  flux at lower energies. For the same reason, the flux is suppressed at higher energies  $E \gtrsim 10$  MeV, such that, for  $E \gtrsim 20$  MeV, the flux lies below the smallest value allowed by the uncertainty on the SFR, see the inset in the left panel.

The dependence on  $z_s$  and  $B_s$  of the final flux is similar to the masses-only varying case. If  $z_s \lesssim 0.1$ , the DSNB is mostly composed of neutrinos that were emitted when their masses and mixing angles were small. On the other hand, if  $z_s \gtrsim 2$ , the largest contribution to the DSNB comes from neutrinos produced with masses and mixing angles similar to the ones observed today. In the latter case, the DSNB will be consistent with standard values. On the other hand, depending on how fast the transition between almost massless neutrinos and the observed mixing pattern occurs, parametrized by B<sub>s</sub>, the flux is enhanced at low energies. If the transition is rather sharp ( $B_s \gtrsim 10$ ), the DSNB is simply the superposition of a nearly massless component coming from SN explosions with  $z > z_s$  and a standard part emitted when  $z < z_s$ . For smaller values of  $B_s$ , the dependence on redshift is smoother, leading to a small variation of the

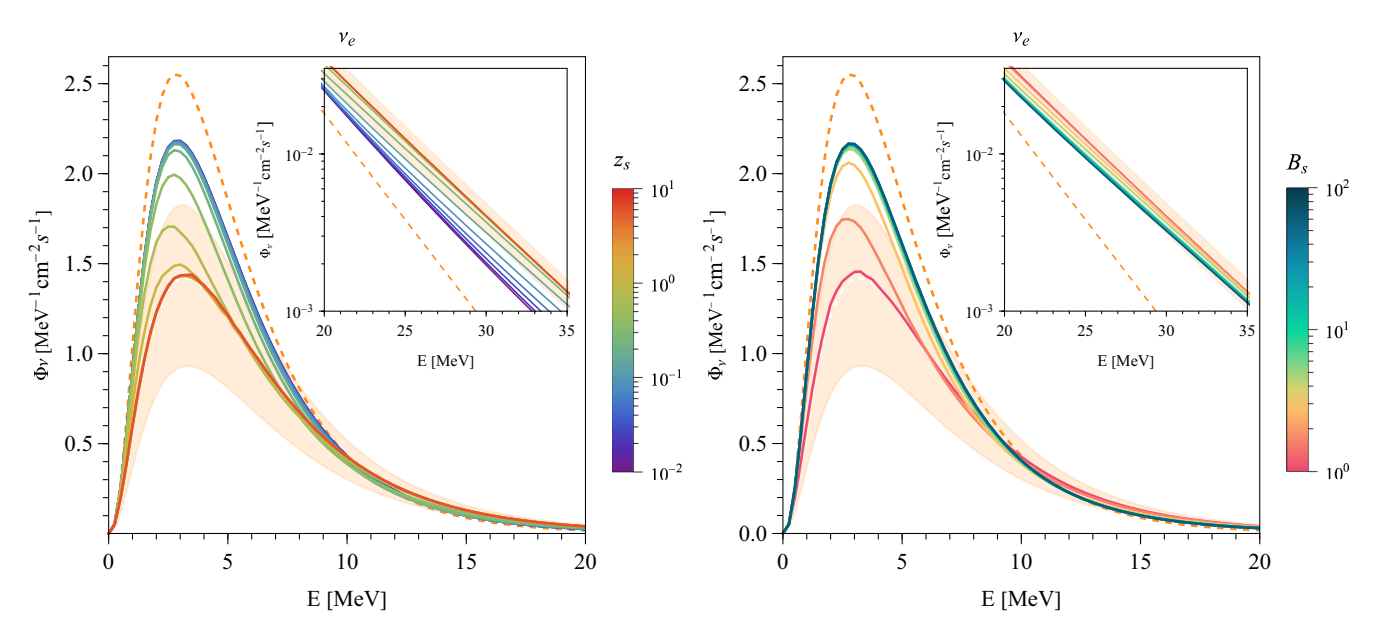


FIG. 8. Left: the DSNB  $\nu_e$  flux as a function of the neutrino energy for different values of  $z_s \in [10^{-2}, 1]$  (rainbow colored) and fixed  $B_s = 5$  and for the standard case (orange) including the star-formation-rate uncertainty (orange band). The dashed orange line indicates the DSNB flux assuming massless neutrinos, i.e.,  $P_{ee}(z) = 1$  for all z. Right: the DSNB  $\nu_e$  flux as a function of the neutrino energy for different values of  $B_s \in [1,100]$  (rainbow colored) and fixed  $z_s = 0.32$  and for the standard case (orange) including the star-formation-rate uncertainty (orange band). The dashed orange line indicates the DSNB flux assuming massless neutrinos, i.e.,  $P_{ee}(z) = 1$  for all z. We assume the normal ordering for the neutrino masses.

masses as a function of redshift. For instance, for  $B_s = 1$ ,  $\Delta m_{ij}^2(z=10)/\Delta m_{ij}^2 \sim 0.02$ , and the propagation in the SN is still adiabatic. In this case, there are no significant changes to the DSNB spectrum.

The  $\bar{\nu}_e$  spectra in this case are virtually unaltered. The MSW adiabatic flavor conversion predicts that  $\overline{P_{ee}} = |U_{e1}|^2$ , value equal to the probability obtained when the mixing angles are small. Since  $\bar{\nu}_e$  would be mostly composed by  $\bar{\nu}_1$ , because the PMNS matrix would be close to diagonal, the predicted antineutrino flux at Earth would be identical to the standard case. As before, a measurement of both neutrinos and antineutrinos from the DSNB would be crucial to test this scenario.

### V. EVENT SPECTRA IN A DUNE-LIKE DETECTOR

The detection of the DSNB is one of the main goals of current and future experiments, including SK and HK [54,55], JUNO [56], and perhaps DUNE [57]. Our results from the last section can be summarized as follows. If the neutrino mass varies as a function of redshift around  $z \sim 1$  and if the neutrino-mass ordering is normal, we expect the DSNB  $\nu_e$  flux to be very different from standard expectations. The DSNB  $\bar{\nu}_e$  flux, on the other hand, is quite indifferent to the potential z dependency of neutrino masses. These two facts point toward a simple strategy for testing the hypothesis that neutrino masses turn on as a function of time. The detection of the DSNB  $\bar{\nu}_e$  flux in experiments like SK and HK<sup>2</sup> can be used to normalize the total flux, thus reducing systematic uncertainties, including those related to uncertainties in the SFR. Meanwhile, data from an experiment like DUNE, which can detect electron neutrinos instead of antineutrinos, can be used to provide information on whether the  $\nu_e$  spectrum is consistent with standard expectations.

Of course, a measurement of the DSNB in either Cherenkov or liquid argon detectors is not an easy task. There are many sources of uncertainty and backgrounds that will impact the search for the DSNB [58]. The measurement of the DSNB flux is bounded from lower energies by the solar neutrino flux, setting a energy threshold of ~16 MeV. From above, this becomes dominated by the atmospheric  $\nu_e$  component at ~40 MeV. Regarding the detector systematic uncertainties, the most relevant are related to the energy reconstruction that are based on the measurement of the electron produced in the neutrino absorption by  $^{40}$ Ar

We compute the number of events at a DUNE-like detector fixing  $B_s = 5$ ,  $z_s = 0.05$ , assuming an exposure of 400 kton yr, and considering as detection channel the process  $\nu_e + {}^{40}\text{Ar} \rightarrow {}^{40}\text{K}^* + e^-$ . As far as other characteristics of the DUNE-like detector, we repeat the assumptions we made in Ref. [19]. Figure 9 depicts event spectra as a

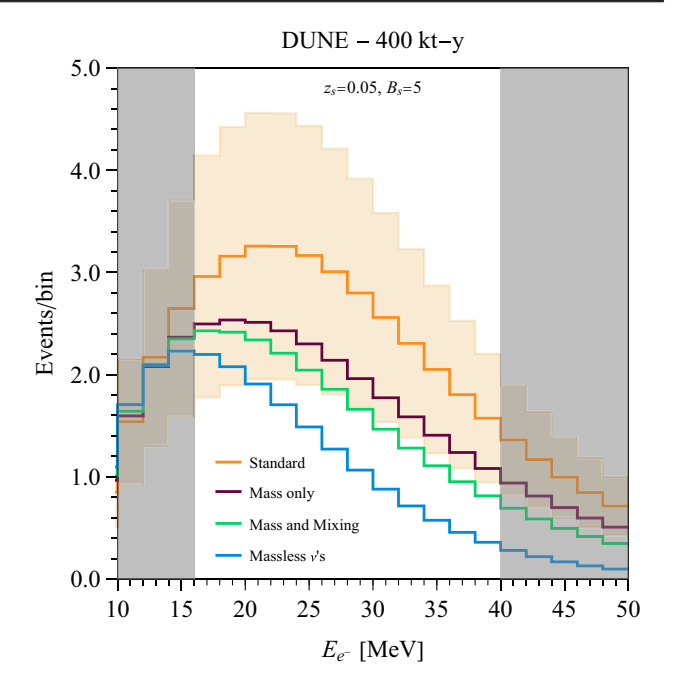


FIG. 9.  $\nu_e$  DSNB event spectra in a DUNE-like detector, assuming 400 kton yr of exposure, as function of the recoil-electron energy. The spectrum in the standard case is in orange, together with the uncertainty associated with the star-formation rate (orange region). Other spectra correspond to the case of mass-varying neutrinos (Tyrian purple), the case where both masses and mixing angles vary (green), for  $z_s = 0.05$  and  $B_s = 5$ , and the case where all neutrino masses are zero (cyan). We assume the normal ordering for the neutrino masses. The gray regions correspond to those where the expected number of background events is dominant.

function of the electron kinetic energy. The standard case is depicted in orange along with the uncertainties associated with our imperfect understanding of the SFR (orange region). We consider the case where only the neutrino masses vary (Tyrian purple) and the one where both the masses and mixing angles vary (green). The blue curve corresponds to the expected  $\nu_e$  flux under the assumption that the neutrinos are massless. The gray bands correspond to regions where background events are expected to be dominant. If the neutrino masses turn on at a finite redshift, the DSNB  $\nu_e$  flux is significantly smaller relative to standard expectations, as observed in the previous section. For  $E_{e^-} \gtrsim 30$  MeV, in the case where both masses and mixing angles vary (green), the flux is expected to lie slightly below the orange-shaded standard region. Figure 9 reveals that a better understanding of systematic uncertainties is crucial to test the hypothesis that the neutrino oscillation parameters is z dependent. As previously mentioned, a high-statistics measurement of the DSNB antineutrino flux should play a decisive role in reducing uncertainties.

Together with the event prediction for the different sets of values of the  $z_s$  and  $B_s$ , we have shown the astrophysical

<sup>&</sup>lt;sup>2</sup>These experiments, along with scintillator experiments, predominantly detect the DSNB via inverse beta decay.

uncertainties related to the SFR. There are other types of uncertainties that can also contribute to modify the expected flux [38]. For instance, there are uncertainties related to the black hole formation from core-collapse SN that mainly affect the high-energy part of the SN neutrino flux. Other uncertainties are related to the contribution of low-mass progenitors like neutron stars. Moreover, we also have uncertainties related to the equation of state, and so on. Those uncertainties will reduce the sensitivity of the DSNB to the neutrino mass. On the other side, the reduced impact that the neutrino-mass variation has over the antineutrino flux, led us to consider that a combined analysis between experiments that measure both components of the flux can reduce the impact of those uncertainties. A detailed analysis, where all the uncertainties that affect the neutrino flux and its measurement, is required in order to determine the statistical significance of the massvarying hypothesis using the DSNB, but such a task lies beyond the scope of this work.

#### VI. CONCLUSIONS

After more than two decades, the mystery surrounding the origin of the neutrino mass persists. A popular direction to pursue is to introduce new physics at high- or very-high-energy scales, but it is clear that very light new physics can also do the job. There is the possibility that the neutrinos are effectively massless at high redshifts and gain masses only recently, at very low redshifts, due to some exotic new physics operating at these scales. Such low-scale physics only affects the evolution of the Universe after photon decoupling and hence is completely compatible with observations of the CMB and other cosmic surveys.

In this work, we propose that imprints of such low redshift neutrino-mass generation can be found on the diffuse supernova neutrino background. The DSNB consists of neutrinos from all past supernovae, since the birth of star formation (redshifts around 5). If neutrino masses are generated at relatively low redshifts, neutrino flavor evolution through the SN is different from standard expectations. These effects can lead to significant changes to the flavor content of the neutrinos arriving at Earth. Using a phenomenological parametrization for the redshift evolution of neutrino masses and mixing angles, we computed the DSNB spectra at Earth. We found that the DSNB  $\nu_e$ spectral shape is sensitive to the epoch of neutrino-mass generation: the peak can be, roughly, larger by up to a factor of 1.5, while the tail can be suppressed, leading to a more pinched spectrum. We also identified scenarios where,

earlier in the history of the Universe, neutrino flavor propagation is completely nonadiabatic inside the SN. Finally, we simulated DSNB event spectra in a DUNElike detector for different hypotheses concerning the time dependency of the neutrino oscillation parameters and demonstrated that redshift-varying neutrino masses and mixing angles can lead to the suppression of the  $\nu_e$  event spectrum. We find that there are circumstances under which effects due to time-dependent oscillation parameters are significant, even if one includes uncertainties associated with our current understanding of the SFR, especially in the higher energy bins. However, there are additional uncertainties that affect the determination of the DSNB flux, such as stellar diversity, microphysical, modeling, and astrophysical uncertainties [38], which in turn may hinder the effect of mass-varying neutrinos. Nevertheless, the concurrent measurement, with enough statistics, of both electron neutrinos and antineutrinos from the DSNB should allow one to make relatively robust claims about the constancy of neutrino masses. This is because we can use the measurement of the  $\bar{\nu}_e$  flux to constrain the aforementioned uncertainties and then contrast with the measurement of the electron-neutrino component.

Measurements of the DSNB are possibly the only way to test scenarios where the mass generation of neutrinos occurred only recently in the history of the Universe. The Super-Kamiokande experiment, doped with gadolinium, is expected to make a compelling discovery of the DSNB within this decade [54]. Future experiments like Hyper-Kamiokande (also doped with gadolinium) are expected to collect a significant sample of DSNB events. On the astrophysical front, we expect the uncertainties on the determination of the DSNB flux to be reduced in the coming decades. As a result, it is exciting to wonder whether a measurement of the DSNB can shed some light on the origin of the neutrino mass.

## ACKNOWLEDGMENTS

We would like to thank Pedro Machado for illuminating discussions on mass-varying neutrinos. I. M.-S., Y. F. P.-G., and M. S. would like thank Northwestern University where part of the work was done. I. M.-S. and Y. F. P.-G. would like to thank the Fermilab theory group where this work started. This work was supported in part by the U.S. Department of Energy (DOE) Award No. de-sc0010143 and in part by the National Science Foundation under Grants No. PHY-1630782 and No. PHY-1748958.

- [1] M. Tanabashi *et al.* (Particle Data Group), Review of particle physics, Phys. Rev. D **98**, 030001 (2018).
- [2] M. Aker et al. (KATRIN Collaboration), Improved Upper Limit on the Neutrino Mass from a Direct Kinematic Method by KATRIN, Phys. Rev. Lett. 123, 221802 (2019).
- [3] M. Aker *et al.*, First direct neutrino-mass measurement with sub-eV sensitivity, Nat. Phys. **18**, 160 (2022).
- [4] I. Esteban, M. C. Gonzalez-Garcia, M. Maltoni, T. Schwetz, and A. Zhou, The fate of hints: Updated global analysis of three-flavor neutrino oscillations, J. High Energy Phys. 09 (2020) 178.
- [5] T. M. C. Abbott *et al.* (DES Collaboration), Dark Energy Survey Year 3 results: Cosmological constraints from galaxy clustering and weak lensing, Phys. Rev. D 105, 023520 (2022).
- [6] N. Aghanim *et al.* (Planck Collaboration), Planck 2018 results. VI. Cosmological parameters, Astron. Astrophys. 641, A6 (2020).
- [7] N. Palanque-Delabrouille, C. Yèche, N. Schöneberg, J. Lesgourgues, M. Walther, S. Chabanier, and E. Armengaud, Hints, neutrino bounds and WDM constraints from SDSS DR14 Lyman-α and Planck full-survey data, J. Cosmol. Astropart. Phys. 04 (2020) 038.
- [8] S. Weinberg, Baryon and Lepton Nonconserving Processes, Phys. Rev. Lett. 43, 1566 (1979).
- [9] A. de Gouvêa, Neutrino mass models, Annu. Rev. Nucl. Part. Sci. 66, 197 (2016).
- [10] R. Fardon, A. E. Nelson, and N. Weiner, Dark energy from mass varying neutrinos, J. Cosmol. Astropart. Phys. 10 (2004) 005.
- [11] G. Krnjaic, P. A. N. Machado, and L. Necib, Distorted neutrino oscillations from time varying cosmic fields, Phys. Rev. D **97**, 075017 (2018).
- [12] A. Dev, P. A. N. Machado, and P. Martínez-Miravé, Signatures of ultralight dark matter in neutrino oscillation experiments, J. High Energy Phys. 01 (2021) 094.
- [13] C. S. Lorenz, L. Funcke, E. Calabrese, and S. Hannestad, Time-varying neutrino mass from a supercooled phase transition: Current cosmological constraints and impact on the  $\Omega_m \sigma_8$  plane, Phys. Rev. D **99**, 023501 (2019).
- [14] G. Dvali and L. Funcke, Small neutrino masses from gravitational  $\theta$ -term, Phys. Rev. D **93**, 113002 (2016).
- [15] C. S. Lorenz, L. Funcke, M. Löffler, and E. Calabrese, Reconstruction of the neutrino mass as a function of redshift, Phys. Rev. D 104, 123518 (2021).
- [16] J. A. Formaggio, A. L. C. de Gouvêa, and R. G. H. Robertson, Direct measurements of neutrino mass, Phys. Rep. 914, 1 (2021).
- [17] C. Lunardini, The diffuse supernova neutrino flux, supernova rate and SN1987A, Astropart. Phys. 26, 190 (2006).
- [18] J. F. Beacom, The diffuse supernova neutrino background, Annu. Rev. Nucl. Part. Sci. **60**, 439 (2010).
- [19] A. de Gouvêa, I. Martinez-Soler, Y. F. Perez-Gonzalez, and M. Sen, Fundamental physics with the diffuse supernova background neutrinos, Phys. Rev. D 102, 123012 (2020).
- [20] Z. Tabrizi and S. Horiuchi, Flavor triangle of the diffuse supernova neutrino background, J. Cosmol. Astropart. Phys. 05 (2021) 011.

- [21] A. Das, Y. F. Perez-Gonzalez, and M. Sen, Neutrino secret self-interactions: A booster shot for the cosmic neutrino background, arXiv:2204.11885.
- [22] H. Zhang *et al.* (Super-Kamiokande Collaboration), Supernova relic neutrino search with neutron tagging at Super-Kamiokande-IV, Astropart. Phys. **60**, 41 (2015).
- [23] K. Abe *et al.* (Super-Kamiokande Collaboration), Diffuse supernova neutrino background search at Super-Kamiokande, Phys. Rev. D **104**, 122002 (2021).
- [24] K. Abe *et al.* (Hyper-Kamiokande Collaboration), Hyper-Kamiokande design report, arXiv:1805.04163.
- [25] F. An *et al.* (JUNO Collaboration), Neutrino physics with JUNO, J. Phys. G **43**, 030401 (2016).
- [26] B. Abi *et al.* (DUNE Collaboration), Deep Underground Neutrino Experiment (DUNE), Far detector technical design report, Volume II DUNE physics, arXiv:2002.03005.
- [27] L. Pattavina, N. Ferreiro Iachellini, and I. Tamborra, Neutrino observatory based on archaeological lead, Phys. Rev. D **102**, 063001 (2020).
- [28] A. M. Suliga, J. F. Beacom, and I. Tamborra, Towards probing the diffuse supernova neutrino background in all flavors, Phys. Rev. D **105**, 043008 (2022).
- [29] S. Baum, F. Capozzi, and S. Horiuchi, Rocks, water and noble liquids: Unfolding the flavor contents of supernova neutrinos, arXiv:2203.12696 [Phys. Rev. D (to be published)].
- [30] A. M. Hopkins and J. F. Beacom, On the normalisation of the cosmic star formation history, Astrophys. J. 651, 142 (2006).
- [31] H. Yuksel, M. D. Kistler, J. F. Beacom, and A. M. Hopkins, Revealing the high-redshift star formation rate with gammaray bursts, Astrophys. J. **683**, L5 (2008).
- [32] S. Horiuchi, J. F. Beacom, and E. Dwek, The diffuse supernova neutrino background is detectable in Super-Kamiokande, Phys. Rev. D **79**, 083013 (2009).
- [33] E. E. Salpeter, The luminosity function and stellar evolution, Astrophys. J. **121**, 161 (1955).
- [34] I. Tamborra, B. Muller, L. Hudepohl, H.-T. Janka, and G. Raffelt, High-resolution supernova neutrino spectra represented by a simple fit, Phys. Rev. D **86**, 125031 (2012).
- [35] K. Mø A. M. Suliga, I. Tamborra, and P. B. Denton, Measuring the supernova unknowns at the next-generation neutrino telescopes through the diffuse neutrino background, J. Cosmol. Astropart. Phys. 05 (2018) 066.
- [36] N. Aghanim *et al.* (Planck Collaboration), Planck 2018 results. VI. Cosmological parameters, Astron. Astrophys. 641, A6 (2020).
- [37] Results from, https://wwwmpa.mpa-garching.mpg.de/ ccsnarchive/.
- [38] D. Kresse, T. Ertl, and H.-T. Janka, Stellar collapse diversity and the diffuse supernova neutrino background, Astrophys. J. 909, 169 (2021).
- [39] H. Duan, G. M. Fuller, J. Carlson, and Y.-Z. Qian, Simulation of coherent non-linear neutrino flavor transformation in the supernova environment. 1. Correlated neutrino trajectories, Phys. Rev. D 74, 105014 (2006).
- [40] S. Hannestad, G. G. Raffelt, G. Sigl, and Y. Y. Y. Wong, Self-induced conversion in dense neutrino gases: Pendulum in flavor space, Phys. Rev. D 74, 105010 (2006); 76, 029901 (E) (2007).

- [41] L. Wolfenstein, Neutrino oscillations in matter, Phys. Rev. D 17, 2369 (1978).
- [42] S. M. Koksbang and S. Hannestad, Constraining dynamical neutrino mass generation with cosmological data, J. Cosmol. Astropart. Phys. 09 (2017) 014.
- [43] A. Berlin, Neutrino Oscillations as a Probe of Light Scalar Dark Matter, Phys. Rev. Lett. 117, 231801 (2016).
- [44] L. Wolfenstein, Neutrino oscillations in matter, Phys. Rev. D 17, 2369 (1978).
- [45] S. P. Mikheyev and A. Y. Smirnov, Resonance amplification of oscillations in matter and spectroscopy of solar neutrinos, II Nuovo Cimento C 9, 17 (1986).
- [46] S. J. Parke, Nonadiabatic Level Crossing in Resonant Neutrino Oscillations, Phys. Rev. Lett. 57, 1275 (1986).
- [47] S. T. Petcov, Exact analytic description of two neutrino oscillations in matter with exponentially varying density, Phys. Lett. B 200, 373 (1988).
- [48] P. I. Krastev and S. T. Petcov, On the analytic description of two neutrino transitions of solar neutrinos in the sun, Phys. Lett. B 207, 64 (1988); 214, 661(E) (1988).
- [49] S. T. Petcov, On the oscillations of solar neutrinos in the sun, Phys. Lett. B **214**, 139 (1988).
- [50] A. Friedland, On the evolution of the neutrino state inside the sun, Phys. Rev. D 64, 013008 (2001).

- [51] T.-K. Kuo and J. T. Pantaleone, Nonadiabatic neutrino oscillations in matter, Phys. Rev. D 39, 1930 (1989).
- [52] A. S. Dighe and A. Yu. Smirnov, Identifying the neutrino mass spectrum from the neutrino burst from a supernova, Phys. Rev. D **62**, 033007 (2000).
- [53] A. Friedland, MSW Effects in Vacuum Oscillations, Phys. Rev. Lett. 85, 936 (2000).
- [54] K. Abe *et al.* (Super-Kamiokande Collaboration), First gadolinium loading to Super-Kamiokande, Nucl. Instrum. Methods Phys. Res., Sect. A **1027**, 166248 (2022).
- [55] K. Abe *et al.* (Hyper-Kamiokande Collaboration), Hyper-Kamiokande design report, arXiv:1805.04163.
- [56] F. An et al. (JUNO Collaboration), Neutrino physics with JUNO, J. Phys. G 43, 030401 (2016).
- [57] B. Abi *et al.* (DUNE Collaboration), Deep Underground Neutrino Experiment (DUNE), Far detector technical design report, Volume I introduction to DUNE, J. Instrum. **15**, T08008 (2020).
- [58] B. Abi et al. (DUNE Collaboration), Deep Underground Neutrino Experiment (DUNE), Far detector technical design report, Volume II: DUNE physics, arXiv:2002.03005.